

# Detecting Multiparticle Entanglement of Dicke States (Supplemental Material)

B. Lücke<sup>1</sup>, J. Peise<sup>1</sup>, G. Vitagliano<sup>2</sup>, J. Arlt<sup>3</sup>, L. Santos<sup>4</sup>, G. Tóth<sup>2,5,6</sup>, C. Klempt<sup>1</sup>

<sup>1</sup>*Institut für Quantenoptik, Leibniz Universität Hannover, Welfengarten 1, D-30167 Hannover, Germany*

<sup>2</sup>*Department of Theoretical Physics, University of the Basque Country UPV/EHU, P.O. Box 644, E-48080 Bilbao, Spain*

<sup>3</sup>*QUANTOP, Institut for Fysik og Astronomi, Aarhus Universitet, 8000 Århus C, Denmark*

<sup>4</sup>*Institut für Theoretische Physik, Leibniz Universität Hannover, Appelstraße 2, D-30167 Hannover, Germany*

<sup>5</sup>*IKERBASQUE, Basque Foundation for Science, E-48011 Bilbao, Spain and*

<sup>6</sup>*Wigner Research Centre for Physics, Hungarian Academy of Sciences, P.O. Box 49, H-1525 Budapest, Hungary*

## S1. ESTIMATION OF VARIANCES

The experimental results of Fig. 3 are based on an estimate of the variance of the total spin of the ensemble. This section shows how these values can be extracted from the raw data. First, the raw data is presented. Second, the statistical treatment for the unbiased estimation of the underlying variance is described. Finally, we show that the variance of  $J_z$  results mainly from number-dependent detection noise.

### A. Measured probability distribution of $J_z$ and $J_\alpha$

The number of atoms in the Zeeman levels is measured by standard absorption imaging with an illumination time of  $70 \mu\text{s}$  and an intensity of  $40 \text{ W/m}^2$ . The absolute number of atoms was calibrated [48] and it was confirmed that shot noise fluctuations are observed for a coherent state [see Fig. 3 (a)]. Without the microwave coupling pulse, a measurement of the number of atoms in the Zeeman levels corresponds to a measurement of  $J_z$ . While an ideal Dicke state would show no fluctuations at all, we record a finite variance. This finite variance may stem from fluctuations of the number of atoms and from noise in the detection system. Figure S1 (a) shows the histogram of all measured values for  $J_z$  with a total number of atoms between 3000 and 7000. The measured distribution is much narrower than the corresponding result for a coherent state. After a  $\frac{\pi}{2}$  microwave pulse, it is possible to record the corresponding histogram in the  $J_x$ - $J_y$ -plane. Since the microwave has an arbitrary phase difference  $\alpha$  from the atomic phases, each measurement projects onto a different axis  $J_\alpha$  in the  $J_x$ - $J_y$ -plane. The histogram in Fig. S1 (b) thus includes measurements along all possible directions. The histogram shows super-shot-noise fluctuations, yielding a large effective spin length  $J_{\text{eff}}$ . The presented data can be used to estimate the second moment of the underlying probability distribution.

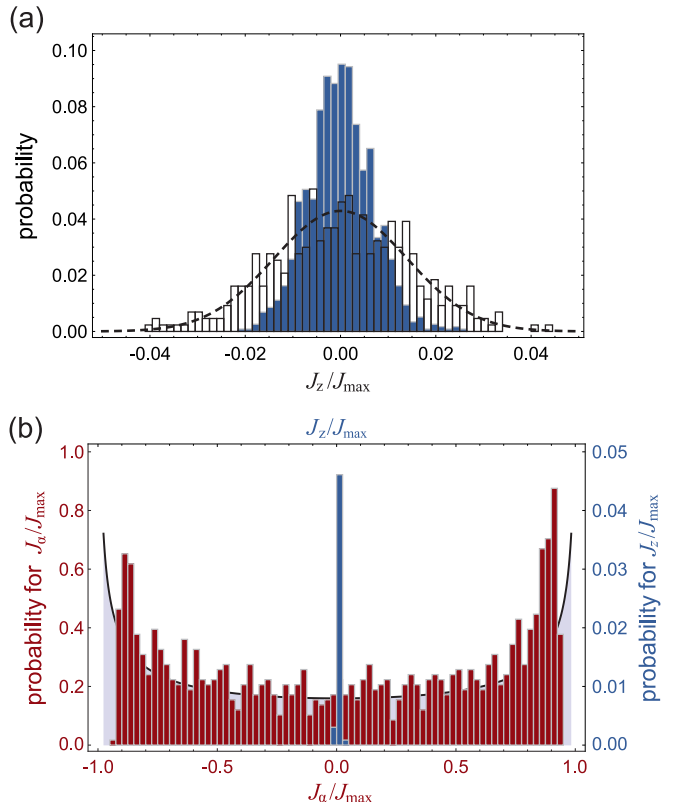


FIG. S1. Histograms of the recorded spin measurements. (a) The accumulated measurements of  $J_z$  are shown for a Dicke-like state (solid blue columns) and a coherent state (open columns). The distribution of the Dicke-like state is much narrower than the distribution of the coherent state. The latter is very close to a binomial distribution with shot noise fluctuations (dashed line). We corrected for a small offset between the two distributions. (b) The accumulated measurements of  $J_\alpha$  are shown for a Dicke-like state (solid red columns). The distribution compares well to the distribution of a perfect Dicke state (solid grey line with shading). It is much wider than the sub-shot-noise distribution of  $J_z$  (solid blue columns).

### B. Unbiased estimation of the second moment of the probability distribution

The measurement process creates a finite set of random numbers  $x_i$  according to a special, non-Gaussian probability function  $P(x)$  [see Fig. S1 (b) as an example].

Such a probability function is well described by its moments  $\mu_1 = \int xP(x)dx$  and  $\mu_k = \int (x - \mu_1)^k P(x)dx$  for  $k \geq 2$ . The second moment  $\mu_2$ , which presents the central quantity of interest within our work, can be estimated straightforwardly from the measurements as shown below. However, the variance of this estimate is more difficult to deduce and has previously been gained from split samples [17]. In this section, we present a formula for an unbiased estimate of this variance (called second moment variance estimator, SMVE), allowing for the calculation of correct error bars for the central result of our work [see Fig. 1 (c)].

For a given sample of  $n$  independent measurements according to the probability function  $P(x)$ , it is possible to calculate the sample moments

$$\begin{aligned} m_1 &= \frac{1}{n} \sum_{i=1}^n x_i, \\ m_2 &= \frac{1}{n} \sum_{i=1}^n (x_i - m_1)^2, \\ m_4 &= \frac{1}{n} \sum_{i=1}^n (x_i - m_1)^4. \end{aligned}$$

The expectation value of  $m_2$  is easily calculated to be

$$\langle m_2 \rangle = \frac{n-1}{n} \mu_2.$$

It is thus possible to define an unbiased estimator for  $\mu_2$ :

$$\hat{\mu}_2 = \frac{n}{n-1} m_2.$$

This estimate shows statistical fluctuations which are described by the variance of  $\hat{\mu}_2$ ,

$$\begin{aligned} \text{var}(\hat{\mu}_2) &= \frac{n^2}{(n-1)^2} \text{var}(m_2) \\ &= \frac{n^2}{(n-1)^2} \left( \langle m_2^2 \rangle - \langle m_2 \rangle^2 \right) \\ &= \frac{n^2}{(n-1)^2} \langle m_2^2 \rangle - \mu_2^2. \end{aligned} \quad (\text{S1})$$

Thus, the problem of finding an estimator for  $\text{var}(\hat{\mu}_2)$  reduces to finding an estimator for  $\mu_2^2$ . Hence, we calculate the expectation values  $\langle m_2^2 \rangle$  and  $\langle m_4 \rangle$  by using augmented and monomial symmetric functions (see Ref. [27] p. 416).

$$\begin{aligned} \langle m_2^2 \rangle &= \frac{(n-1)^2}{n^3} \mu_4 + \frac{(n-1)(n^2 - 2n + 3)}{n^3} \mu_2^2 \\ \langle m_4 \rangle &= \frac{n^3 - 4n^2 + 6n - 3}{n^3} \mu_4 + \frac{3(n-1)(2n-3)}{n^3} \mu_2^2 \end{aligned}$$

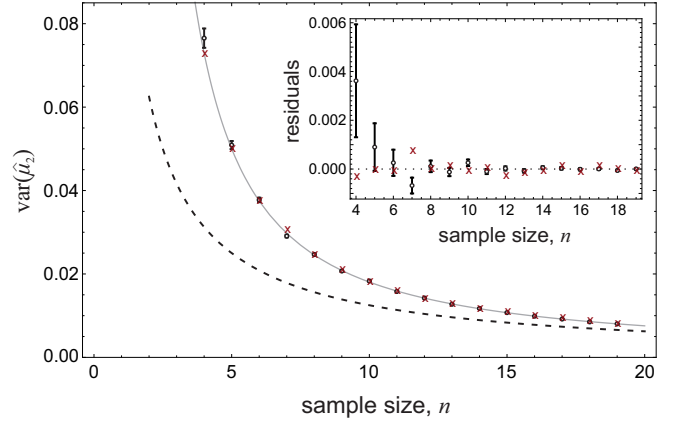


FIG. S2. Application of the SMVE to generated random numbers. We have generate random numbers according to a probability function  $P(x)$ . For each sample size  $n$ , we have applied the SMVE to  $10^4$  samples. The open circles present the mean of the calculated SMVEs with their statistical uncertainties. These results compare well to the directly calculated variance of the  $10^4$  sample variances (red solid dots). It is statistically equal to the prediction  $\text{var}(\hat{\mu}_2) = \frac{1}{n} \mu_4 - \frac{n-3}{n(n-1)} \mu_2^2$  and completely incompatible with the naive guess  $\text{var}(\hat{\mu}_2) \approx \frac{1}{n} (\mu_4 - \mu_2^2)$  (dashed line).

This linear system of equations can be solved to yield an estimator for  $\mu_2^2$ . By substituting this in Eq. (S1), we obtain the final result for the SMVE,

$$\text{var}(\hat{\mu}_2) = \frac{n}{(n-3)(n-2)} m_4 - \frac{n(n^2-3)}{(n-3)(n-2)(n-1)^2} m_2^2.$$

The SMVE allows for a direct calculation of the error bars from the moments of the recorded sample without any assumption on the shape of the probability distribution.

Figure S2 shows the result of a Monte-Carlo simulation to demonstrate the application of the SMVE. We generate random numbers according to a probability function  $P(x) = \frac{1}{\pi} \sqrt{\frac{1}{1-x^2}}$ , similar to Fig. S1 (b), and accumulate samples of variable size. The SMVE is applied to  $10^4$  samples of each size, yielding estimates for  $\text{var}(\hat{\mu}_2)$ . Figure S2 shows that these estimates approximate the directly calculated variance of the  $10^4$  sample variances very well. It is statistically equal to the prediction gained solely from the shape of the probability distribution.

In summary, the statistical treatment allows for a correct evaluation of the second moment of the underlying probability function and its uncertainty.

### C. Estimation of the detection noise

The second moment gained from the experimental measurements via the statistical treatment above is a

combination of the variance  $(\Delta J_z)^2$  of the atomic many-particle state and the detection noise. The detection noise comprises an atom-independent part which is dominated by the photoelectron shot noise on the camera pixels and an atom-dependent part. The atom-independent noise was measured continuously during the data acquisition by analysing images without atoms. Since we are interested in an estimate for  $(\Delta J_z)^2$ , the data in Fig. 3 (a) are corrected for the atom-independent noise.

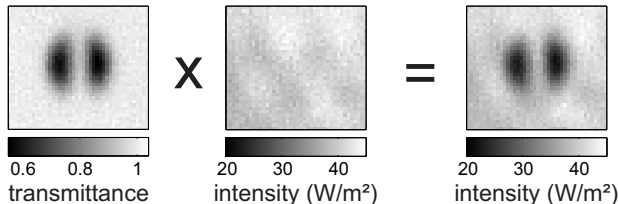


FIG. S3. Creation of an artificial absorption image. The optical transmittance of an idealized atomic cloud is calculated from an average of many experimental absorption images. A typical detection image without atoms is multiplied by the optical transmittance to gain a synthetic absorption image with adjustable number of atoms.

The atom-dependent detection noise results from fluctuations of the photoelectrons counted on the camera pixels which are stronger at a large number of atoms. Additionally, a change in the number of counted photoelectrons has a larger effect on the estimated number of atoms at high column densities resulting in an increased sensitivity at a large number of atoms. This noise source is not independent of the atomic noise and it is thus not legitimate to subtract it. Nevertheless, we estimate the approximate strength of these fluctuations for comparison with our results. For this purpose, we calculate the mean optical transmittance from many experimental realizations (see Fig. S3) to approximate an ideal atomic cloud without atom number fluctuations. This optical transmittance image is adjusted to represent clouds with different numbers of atoms. We synthesize absorption images by multiplying empty detection images with the gained transmittance images. These artificial absorption images provide a measure of the atom-dependent detection noise since they do not contain any atom number fluctuations by construction. The resulting estimate for the atom-dependent detection noise is shown in Fig. 3 (a) (dashed line). Although it underestimates the effect of photoelectron shot noise for strongly depleted absorption images, it nevertheless explains the major part of the measured variance  $(\Delta J_z)^2$ .

## S2. BOUNDARIES FOR GENUINE $k$ -PARTICLE ENTANGLEMENT

This section presents a method for the determination of the entanglement depth based on the measurement of  $\langle J_x^2 + J_y^2 \rangle$  and  $(\Delta J_z)^2$ . With this method, we determine the allowed regions for  $k$ -particle entanglement in Fig. 1 (c). Section S2 A provides a numerical method to calculate the boundaries. In Sec. S2 B, we present the entanglement criterion with a closed formula, and we discuss that it applies to pure states, mixed states and mixed states with a varying particle number. Finally, Sec. S2 C presents a comparison with the original spin-squeezing criterion of Ref. [25]. We show that our criterion detects a larger entanglement depth for extreme spin-squeezed states in the presence of minimal noise.

### A. Numerical determination of the boundaries

The following numerical method can be used to determine the allowed region in the  $(\langle J_x^2 + J_y^2 \rangle, (\Delta J_z)^2)$ -space for quantum states with at most  $k$ -particle entanglement for a given particle number  $N$  [28]. We consider states of the form

$$|\Psi\rangle = \otimes_{n=1}^M |\psi^{(n)}\rangle, \quad (\text{S2})$$

where  $|\psi^{(n)}\rangle$  is the state of the  $n$ th non-separable subset containing  $k_n$  qubits and  $k_n \leq k$ . In total, there are  $M$  non-separable subsets. Here, “qubit” refers to individual pseudo-spin- $\frac{1}{2}$  atoms in the experiment. We define the collective operators

$$J_l := \sum_{n=1}^M j_l^{(n)}$$

for  $l = x, y, z$ , where  $j_l^{(n)}$  denotes the components of the  $k_n$ -particle spin operators and act on the  $n$ th non-separable subset of qubits. Note that we consider  $k_n = k$  in the main text, whereas here, we extend our discussion to the general case  $k_n \leq k$ .

The total variance  $(\Delta J_z)^2$  is given by the sum of the variances of the  $k_n$ -particle spin operators

$$(\Delta J_z)^2 = \sum_n (\Delta j_z^{(n)})^2. \quad (\text{S3})$$

On the other hand, for a state of the form (S2)

$$\begin{aligned} \langle J_x^2 + J_y^2 \rangle &= \sum_n \left( \langle j_x^{(n)} \rangle^2 + \langle j_y^{(n)} \rangle^2 \right) \\ &+ \sum_{m \neq n} \left( \langle j_x^{(m)} \rangle \langle j_x^{(n)} \rangle + \langle j_y^{(m)} \rangle \langle j_y^{(n)} \rangle \right). \end{aligned}$$

Since for non-negative values  $\{x_l\}_{l=1}^L$  and positive integer  $L$  we have

$$\sum_{l \neq m} x_l x_m \leq (L-1) \sum_l x_l^2,$$

we obtain

$$\begin{aligned} \langle J_x^2 + J_y^2 \rangle &\leq \sum_n \left( \langle j_x^{(n)} \rangle^2 + \langle j_y^{(n)} \rangle^2 \right) \\ &+ (M-1) \sum_n \left( \langle j_x^{(n)} \rangle^2 + \langle j_y^{(n)} \rangle^2 \right). \end{aligned} \quad (\text{S4})$$

For simplicity, we assume that  $N$  is divisible by  $k$ . In this case, states of the form

$$|\Psi\rangle = |\psi\rangle^{\otimes \frac{N}{k}} \quad (\text{S5})$$

saturate the inequality (S4), where  $|\psi\rangle$  is a  $k$ -qubit state. Due to convexity arguments, it is sufficient to look for states of the form (S5) to calculate the boundary points. A boundary point can be obtained for a given  $X = (\Delta J_z)^2$  from

$$\begin{aligned} \langle J_x^2 + J_y^2 \rangle(X) &= \max_{|\Psi\rangle, \frac{N}{k} (\Delta j_z)^2 = X} \left[ \frac{N}{k} \langle j_x^2 + j_y^2 \rangle_{|\psi\rangle} \right. \\ &\left. + \left( \frac{N}{k} - 1 \right) \frac{N}{k} \left( \langle j_x \rangle_{|\psi\rangle}^2 + \langle j_y \rangle_{|\psi\rangle}^2 \right) \right]. \end{aligned} \quad (\text{S6})$$

Thus, a constrained optimization for a given  $(\Delta j_z)^2_{|\psi\rangle}$  over  $|\psi\rangle$  has to be performed. This can be simplified further as follows. For even  $k$ , the states at the boundary can be sought in the form (S5), where  $|\psi\rangle$  is the ground state of the spin-squeezing Hamiltonian

$$h(\lambda) = j_z^2 - \lambda j_x. \quad (\text{S7})$$

Thus, an optimal state  $|\psi\rangle$  is obtained from spin squeezing [25]. Note that the ground state of  $h(0)$  is degenerate. In this case, the symmetric ground state has to be chosen, i.e., the symmetric Dicke state with  $\langle j_z \rangle = 0$ .

Hence, the boundary points can be obtained for even  $k$  as a function of a single real parameter  $\lambda$  as

$$\begin{aligned} \langle J_x^2 + J_y^2 \rangle(\lambda) &= \left[ \frac{N}{k} \langle j_x^2 + j_y^2 \rangle_{|\psi\rangle(\lambda)} \right. \\ &\left. + \left( \frac{N}{k} - 1 \right) \frac{N}{k} \left( \langle j_x \rangle_{|\psi\rangle(\lambda)}^2 + \langle j_y \rangle_{|\psi\rangle(\lambda)}^2 \right) \right], \\ (\Delta J_z)^2(\lambda) &= \frac{N}{k} (\Delta j_z)^2_{|\psi\rangle(\lambda)}, \end{aligned}$$

where  $|\psi\rangle(\lambda)$  is the ground state of  $h(\lambda)$ . This also means that states of the form  $|\psi\rangle^{\otimes \frac{N}{k}}(\lambda)$  correspond to points on the boundary. Since  $\langle j_z \rangle_{|\psi\rangle(\lambda)} = 0$ , we have  $\langle J_z \rangle = 0$  for the states on the boundary mentioned above. Any state beyond the boundary is at least  $(k+1)$ -particle entangled.

## B. Proof for general states with a large number of particles

In the previous section, we have presented a numerical method to calculate the boundary for  $k$ -particle entangled states assuming that the state is a tensor product of  $k$ -qubit pure states and the particle number is fixed. It is possible to prove that these boundaries are valid for general states (S2) with  $k_n \leq k$ .

To obtain a closed formula for the boundary, we employ the definition [25]

$$F_j(X) := \frac{1}{j} \min_{\langle j_x \rangle = X} (\Delta j_z)^2.$$

The spin-squeezing criterion for  $k$ -particle entangled states is given as

$$(\Delta J_z)^2 \geq J_{\max} F_{\frac{k}{2}} \left( \frac{\sqrt{\langle J_x \rangle^2 + \langle J_y \rangle^2}}{J_{\max}} \right). \quad (\text{S8})$$

Equation (S8) is valid for any tensor product of states of the form (S5) with  $k_n \leq k$  [25, S3].

Moreover, for pure  $k$ -particle entangled states it is straightforward to show that

$$\langle J_x^2 + J_y^2 \rangle \leq J_{\max} \left( \frac{k}{2} + 1 \right) + \langle J_x \rangle^2 + \langle J_y \rangle^2. \quad (\text{S9})$$

Hence, using the properties of  $F_j(X)$ , for states with  $k$ -particle entanglement,

$$(\Delta J_z)^2 \geq J_{\max} F_{\frac{k}{2}} \left( \frac{\sqrt{\langle J_x^2 + J_y^2 \rangle - J_{\max} \left( \frac{k}{2} + 1 \right)}}{J_{\max}} \right) \quad (\text{S10})$$

holds. Naturally, we can use the formula only if the expression under the square root is positive. Otherwise, the lower bound on  $(\Delta J_z)^2$  is trivially zero. For large  $N$  and  $k \ll N$ , the first term under the square root in Eq. (S10) is  $\sim N^2$ , while the second one is  $\sim N$ . Thus, we obtain approximately

$$(\Delta J_z)^2 \gtrsim J_{\max} F_{\frac{k}{2}} \left( \frac{\sqrt{\langle J_x^2 + J_y^2 \rangle}}{J_{\max}} \right). \quad (\text{S11})$$

Note that, since  $F_j(x) \leq \frac{1}{2}$ , a sub-Poissonian variance, i.e.,  $(\Delta J_z)^2 < \frac{N}{4}$  is required to detect multi-particle entanglement.

The inequality (S10) can be used to quantify the entanglement depth of pure states. It gives the same boundary for  $k$ -particle entangled states as the method of Sec. S2 A. It can also be shown that our criterion holds not only for pure states, but also for general mixed states [29]. Moreover, it can be generalized to the experimentally important case of mixed states with a fluctuating total number of particles. Since the total proof exceeds the scope of this publication, it will be published elsewhere [30].

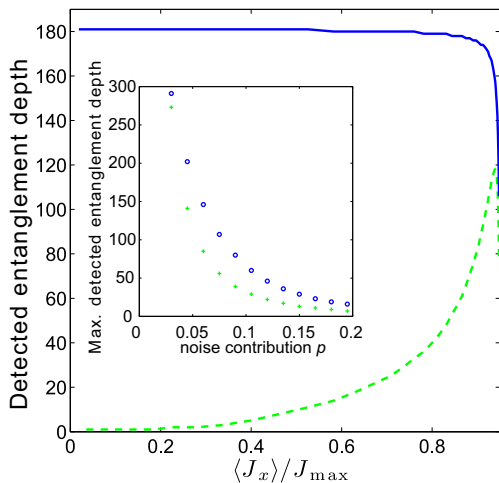


FIG. S4. Comparison with the spin-squeezing criterion. The graph shows the entanglement depth detected by the condition (S10) (solid line) and the spin-squeezing condition (S8) (dashed line) for  $N = 4000$  spin- $\frac{1}{2}$  particles with additive white noise to account for imperfections. For states that are not completely polarized, Eq. (S10) detects a considerably larger entanglement depth. The inset shows that the maximal detected entanglement depth depending on the noise contribution is larger for our criterion (circles) than for the spin-squeezing criterion (crosses) if some very small noise is present.

### C. Comparison with the spin-squeezing criterion

Our criterion reliably detects the entanglement depth of Dicke states. In particular, it detects the symmetric Dicke state with  $\langle J_l \rangle = 0$  for  $l = x, y, z$  as fully  $N$ -particle entangled, since the inequality (S10) with  $k = N - 1$  is violated. In this section, we show that our criterion is also valuable for the evaluation of spin-squeezed states, since it outperforms the criterion of Ref. [25] in the presence

of noise.

In order to compare the performance of the two criteria, we consider the ground states of the spin-squeezing Hamiltonian

$$H(\Lambda) = J_z^2 - \Lambda J_x, \quad (\text{S12})$$

for  $N = 4000$  spin- $\frac{1}{2}$  particles. For  $\Lambda = \infty$ , the ground state is fully polarized. For  $\Lambda = 0$ , it is the symmetric Dicke state. In principle, such states are detected by the spin-squeezing criterion of Ref. [25] as fully  $N$ -particle entangled for all  $\Lambda > 0$ . However, this statement only holds for ideal pure states. In experimentally realistic situations, small noise contributions are always expected, especially for the case of large numbers of particles as considered here. While the criterion of Ref. [25] becomes extremely sensitive to noise for strongly squeezed states, our criterion is much more robust.

We account for these small noise contributions by mixing the density matrix of the ideal spin-squeezed state  $\rho_{\text{id}}$  with a noisy state  $\rho_{\text{n}}$ . The noisy state is chosen such that each atom is in an incoherent 50/50 mixture of its two spin states. For a quantitative comparison, we estimate the entanglement depth of the state  $\rho = (1 - p)\rho_{\text{id}} + p\rho_{\text{n}}$  with a noise contribution of  $p = 0.05$ . Fig. S4 shows the detected entanglement depth for the spin-squeezing criterion (S8) and our criterion (S10). For strongly squeezed states, where  $\langle J_x \rangle \ll J_{\max}$ , our criterion detects a large entanglement depth, while the result of the method described in Ref. [25] tends to zero. The robustness against noise exhibited in this example is a general property and is independent of the exact type of noise.

In summary, our criterion detects the entanglement depth of both spin-squeezed states and more general states in experimentally realistic situations. Most prominently, it is ideally suited for the characterization of Dicke states, as produced in our experiments.